

Non-Markovian dynamics in atom-laser outcoupling from a double-well Bose-Einstein condensate

C. Lazarou¹, G. M. Nikolopoulos², P. Lambropoulos^{2,3}

¹ Department of Physics and Astronomy, University of Sussex, Brighton BN1 9QH, United Kingdom

² Institute of Electronic Structure and Laser, FORTH, P. O. Box 1527, Heraklion 711 10, Crete, Greece

³ Department of Physics, University of Crete, P. O. Box 2208, Heraklion 71003, Crete, Greece

Abstract. We investigate the dynamics of a continuous atom laser based on the merging of independently formed atomic condensates. In a first attempt to understand the dynamics of the system, we consider two independent elongated Bose-Einstein condensates which approach each other and focus on intermediate inter-trap distances so that a two-mode model is well justified. In the framework of a mean-field theory, we discuss the quasi steady-state population of the traps as well as the energy distribution of the outcoupled atoms.

PACS numbers: 03.65.Yz, 03.75.Pp

1. Introduction

The theory of quantum dissipative systems, and in particular those in which structured reservoirs are involved, represents a currently active field of research in a rather broad and varied context [1]. The fundamental challenge in problems involving this type of reservoir stems from the inapplicability of the Born and Markov approximations, normally valid for a reservoir with a smooth density of states, coupled weakly to a quantum system with few degrees of freedom. As a result, the so-called pole approximation which leads to the elimination of the reservoir degrees of freedom can not be adopted. On the other hand, there are no established approaches of general use capable of addressing all problems of this type. The situation is further complicated by the large variety of and seemingly unrelated physical contexts in which such problems may appear. The mathematical structure of the density of states of the reservoir and the strength of the coupling to the quantum system are the determining factors and source of difficulty. Actually, their combination determines the so-called spectral response whose form in each case sets the rules as to which approach may be helpful.

The theoretical description of what is known as atom laser represents a most recent example of this class of problems. In fact, the features that make this problem non-Markovian resemble those of an excited atom inside a material with a photonic bandgap [2]; even though the underlying physics is rather different. In analogy to optical lasers, atom lasers can be obtained by outcoupling atoms from a trapped Bose-Einstein condensate (BEC) to free space. The most crucial prerequisite for the realization of a continuous atom laser is the pumping mechanism replenishing the trapped condensate as atoms are outcoupled from it. A number of sophisticated techniques have been proposed to this end [3], and most of them rely on optical pumping between various internal and external atomic states. However, none of these techniques has been able to overcome intrinsic losses in the system and achieve laser action. Up to date, perhaps the most promising scheme towards the realization of a continuous source of condensed atoms was demonstrated by Chikkatur *et al.* [4], and relies on the use of optical tweezers for the transport and the merging of independently produced BECs.

A large number of theoretical models have been used in studies of atom lasers which rely mainly on Born-Markov master equations [5, 6] and Gross-Pitaevskii theory [7, 8, 9, 10, 11, 12]. In either case, the models hold only under certain operating conditions. For instance, it is well known that for experimentally achievable parameters atom lasers may exhibit non-Markovian dynamics [13, 14], which cannot be described in the framework of Born-Markov approximations. Besides, inclusion of non-Markovian effects in the Gross-Pitaevskii theory is a rather difficult task. Hence, investigations of atom-laser dynamics beyond Born and Markov approximations have been mainly performed in the framework of a particularly simple model involving a single-mode condensate (trap mode) coherently coupled to a continuum of free-space modes [13, 15, 16, 17, 18, 19, 20, 21].

Motivated by the experiments of Chikkatur *et al.* [4], in the present work we extend these studies to a two-mode scenario. In particular, we consider two independent BECs consisting of a large number of bosonic atoms cooled into the lowest eigenmode of the corresponding trap. To account for the merging process, the two traps are brought together, while atoms are coherently outcoupled from one of the BECs only. We focus on an intermediate stage of the merging process where the separation of the two traps is so large that, on the one hand a two-mode model can

be adopted, while on the other hand a coherent Josephson coupling is established between the two BECs. Our purpose is to investigate how the presence of the second trap mode affects the dynamics of the atom laser and in particular the distribution of the outcoupled atoms.

2. The system

Our system (see figure 1) consists of two independently prepared elongated BECs (A and B) and let N be the total number of atoms in the system. The two traps are initially far apart and each BEC experiences only its local potential $V_{A(B)}^{(L)}(\mathbf{r})$, while only the lowest level of each trap (condensate mode) is populated. To allow for the merging of the two BECs, the two traps are brought together along one of the tightly confining radial directions. Simultaneously, atoms are outcoupled coherently from BEC A, by applying external electromagnetic fields. In this section we describe in detail the modeling of the system used throughout this work.

2.1. Double-well potential

Transport of BECs can be realized using optical tweezers which are produced by focused laser beams and offer limited trap volume and depth. Hence, during the merging process the two BECs can be brought as close as the traps' beam waist, before they start affecting each other. To be consistent with the experimental setup for BEC merging [4] as well as related theoretical work [22, 23], we will assume two nearly identical axially symmetric harmonic traps with confining frequencies ω_z and $\omega_x = \omega_y = \omega_\perp$. Trap B is moving towards trap A along the radial direction x (see figure 1), and the global potential experienced by the trapped atoms can be modeled by a time-dependent double-well potential of the form,

$$V_t^{(G)}(\mathbf{r}, t) = \frac{1}{2}m\omega_x^2 \left[\left| x - \frac{s(t)}{2} \right| - \frac{s(t)}{2} \right]^2 + \frac{1}{2}m\omega_y^2 y^2 + \frac{1}{2}m\omega_z^2 z^2, \quad (1)$$

where m is the atomic mass. According to (1), the harmonic potential remains unaffected in both y and z directions, while along the merging direction we have a double well potential which at any time t , exhibits two minima at $x = 0$ and $x = s(t)$ (see left inset of figure 1). The distance between the two dips decreases with time and at the end of the merging (i.e., at $t = t_m$) we have complete overlap.

Besides the merging time-scale t_m , the details of the motion of trap B are not of great importance [4, 22, 23]. The crucial point is that the BEC merging must be adiabatic so that any kind of excitations in the system are suppressed. To this end, first of all the transport of the BECs must take place on a time scale much larger than the characteristic time scale of excitations along the merging direction i.e., $t_m \gg \omega_x^{-1}$ [22, 23]. Although this condition can be easily satisfied in a typical merging experiment [4], it does not ensure adiabaticity with respect to the time-scale of interatomic interactions [22]. Nevertheless, as long as $NU_{tt}t_m \gg 2\hbar V_{\text{mode}}$, where U_{tt} is the strength of the interactions and V_{mode} is the effective mode volume for each trap, it has been shown that only low-lying eigenstates of the Hamiltonian may be populated during the merging [22]. As a result, at the end of the process one obtains a large single-mode BEC fraction with a unique relative phase.

The local potentials centered at $x = 0$ and $x = s(t)$, are readily obtained from equation (1)

$$\begin{aligned} V_A^{(L)}(\mathbf{r}) &= \frac{1}{2}m(\omega_x^2 x^2 + \omega_y^2 y^2 + \omega_z^2 z^2), \\ V_B^{(L)}(\mathbf{r}, t) &= \frac{1}{2}m\{\omega_x^2 [x - s(t)]^2 + \omega_y^2 y^2 + \omega_z^2 z^2\}. \end{aligned} \quad (2)$$

In the case of an ideal bosonic gas, the wavefunction of the local ground states $|A\rangle$ and $|B\rangle$, corresponding to $V_A^{(L)}(\mathbf{r})$ and $V_B^{(L)}(\mathbf{r})$ respectively, have the well known Gaussian-like profile i.e.,

$$\begin{aligned} \varphi_A(\mathbf{r}) \equiv \langle A | \mathbf{r} \rangle &= \frac{1}{\pi^{3/4} l_z^{1/2} l_\perp} \exp \left[-\frac{1}{2} \left(\frac{x^2 + y^2}{l_\perp^2} + \frac{z^2}{l_z^2} \right) \right], \\ \varphi_B(\mathbf{r}, t) \equiv \langle B | \mathbf{r} \rangle &= \frac{1}{\pi^{3/4} l_z^{1/2} l_\perp} \exp \left\{ -\frac{1}{2} \left[\frac{[x - s(t)]^2 + y^2}{l_\perp^2} + \frac{z^2}{l_z^2} \right] \right\}. \end{aligned} \quad (3)$$

The characteristic harmonic oscillator length l_ζ is defined as $l_\zeta \equiv \sqrt{\hbar/m\omega_\zeta}$ for $\zeta \in \{x, y, z\}$, while $l_\perp = l_x = l_y$. As we will see later on, these Gaussian-like profiles enable us to obtain analytic expressions for most of the parameters characterizing the dynamics of the system. From now on, for the sake of brevity we simply write $\varphi_B(\mathbf{r})$ instead of $\varphi_B(\mathbf{r}, t)$.

2.2. Trapped atoms

The many-body Hamiltonian describing the dynamics of the trapped atoms is given by [9, 24, 25]

$$\hat{\mathcal{H}}_t = \int d\mathbf{r} \hat{\Psi}_t^\dagger(\mathbf{r}) \left[-\frac{\hbar^2}{2m} \nabla^2 + V_t^{(G)}(\mathbf{r}, t) \right] \hat{\Psi}_t(\mathbf{r}) + \frac{U_{tt}}{2} \int d\mathbf{r} \hat{\Psi}_t^\dagger(\mathbf{r}) \hat{\Psi}_t^\dagger(\mathbf{r}) \hat{\Psi}_t(\mathbf{r}) \hat{\Psi}_t(\mathbf{r}), \quad (4)$$

where $\hat{\Psi}_t(\mathbf{r})$ is the annihilation field operator for the trapped atoms with

$$\left[\hat{\Psi}_t(\mathbf{r}), \hat{\Psi}_t^\dagger(\mathbf{r}') \right] = \delta(\mathbf{r} - \mathbf{r}'), \quad \left[\hat{\Psi}_t(\mathbf{r}), \hat{\Psi}_t(\mathbf{r}') \right] = 0. \quad (5)$$

The quantity $U_{tt} = 4\pi\hbar^2 a_{tt}/m$ measures the strength of the interparticle interaction between trapped atoms, while a_{tt} is the corresponding s -wave scattering length.

At $t = 0$, each BEC experiences only its local potential $V_{A(B)}^{(L)}$ as the two traps are well separated, and only the lowest level of each trap (condensate mode) is populated. We may expand therefore the field operator at $t = 0$ as $\hat{\Psi}_t(\mathbf{r}, 0) = \varphi_A(\mathbf{r})\hat{a}(0) + \varphi_B(\mathbf{r})\hat{b}(0)$, where $\varphi_A(\mathbf{r})$ and $\varphi_B(\mathbf{r})$ are the ground-state wavefunctions for the traps A and B, respectively [9, 24, 25]. The corresponding bosonic annihilation operators are denoted by \hat{a} and \hat{b} and satisfy the standard commutation relations i.e., $[\hat{d}_i, \hat{d}_j^\dagger] = \delta_{i,j}$, for $\hat{d}_1 = \hat{a}$ and $\hat{d}_2 = \hat{b}$.

To be consistent with the experiment [4], we will assume that during the merging the atomic density profiles follow adiabatically the movement of the traps. The condensate wavefunctions start overlapping in space as the two traps approach each other and a Josephson-type tunneling is established between the two BECs. If the position uncertainty in the ground state of the traps is much smaller than the separation of the minima of the global potential $V_t^{(G)}(\mathbf{r}, t)$ i.e., if

$$l_x \ll \sqrt{2}s, \quad (6)$$

the overlap (and thus the Josephson coupling) is small enough so that only the ground states of the traps are relevant. In first-order perturbation theory, the corresponding local ground-state wavefunctions $\varphi_{A(B)}(\mathbf{r})$ are orthogonal and describe faithfully BEC A and B, at any time $0 < t \ll t_m$ [25]. Hence, under such conditions we may still expand the field operator at times $0 < t \ll t_m$ as [9, 24, 25]

$$\hat{\Psi}_t(\mathbf{r}, t) = \varphi_A(\mathbf{r})\hat{a}(t) + \varphi_B(\mathbf{r})\hat{b}(t), \quad (7)$$

and the many-body Hamiltonian (4) reduces to the standard two-mode model

$$\hat{\mathcal{H}}_t(t) = \hbar\omega_A\hat{a}^\dagger\hat{a} + \hbar\omega_B\hat{b}^\dagger\hat{b} + \hbar J\hat{a}^\dagger\hat{b} + \hbar J^*\hat{b}^\dagger\hat{a} + \hbar\kappa_A\hat{a}^\dagger\hat{a}^\dagger\hat{a}\hat{a} + \hbar\kappa_B\hat{b}^\dagger\hat{b}^\dagger\hat{b}\hat{b}, \quad (8)$$

where the coefficients are given by

$$\omega_j(t) = \frac{1}{\hbar} \int d\mathbf{r} \varphi_j^*(\mathbf{r}) L_t \varphi_j(\mathbf{r}), \quad \kappa_j = \frac{U_{tt}}{2\hbar} \int d\mathbf{r} |\varphi_j(\mathbf{r})|^4, \quad J(t) = \frac{1}{\hbar} \int d\mathbf{r} \varphi_A^*(\mathbf{r}) L_t \varphi_B(\mathbf{r}), \quad (9)$$

with

$$L_t(t) = -\frac{\hbar^2}{2m} \nabla^2 + V_t^{(G)}(\mathbf{r}, t). \quad (10)$$

In deriving equation (8) we have neglected higher-order cross-interaction terms involving integrands of the form $|\varphi_i(\mathbf{r})|^2 |\varphi_j(\mathbf{r})|^2$, $[\varphi_i^*(\mathbf{r}) \varphi_j(\mathbf{r})]^2$, and $|\varphi_j(\mathbf{r})|^2 \varphi_i(\mathbf{r}) \varphi_j^*(\mathbf{r})$.

Condition (6) itself does not justify completely the use of the two-mode model. In addition we have to guarantee that the effect of interatomic interactions on the ground-state properties of the two wells is small i.e., that $\hbar(\omega_x \omega_y \omega_z)^{1/3} \gg N \kappa_j$ [25]. For such weakly-interacting bosonic gases, the ground-state wavefunctions are well approximated by equations (3). The Gaussian profile of the wavefunctions enables us to evaluate analytically all of the integrals (9) obtaining for the coefficients entering the Hamiltonian $\hat{\mathcal{H}}_t$

$$\omega_j = \omega_o, \quad \kappa_j = \kappa, \quad J = J^*, \quad (11)$$

where

$$\omega_o(t) = \omega_z \left[\frac{1}{2} + \frac{1}{\lambda} + \frac{\eta^2}{\lambda} \text{Erfc}(\eta) - \frac{\eta}{\lambda \sqrt{\pi}} e^{-\eta^2} \right], \quad (12)$$

$$J(t) = \omega_z \left(\frac{1}{2} + \frac{1}{\lambda} - \frac{\eta}{\lambda \sqrt{\pi}} \right) e^{-\eta^2}, \quad (13)$$

$$\kappa = \frac{\hbar a_{tt}}{\lambda m \sqrt{2\pi} l_z^3}, \quad (14)$$

while $\text{Erfc}(\eta)$ is the complementary error function and we have introduced the dimensionless quantities $\eta(t) = s(t)/(2l_x)$ and $\lambda = \omega_z/\omega_x$. Condition $\hbar(\omega_x \omega_y \omega_z)^{1/3} \gg N \kappa_j$ thus yields the following upper bound on the total number of atoms we may consider

$$N \ll \lambda^{1/3} \sqrt{2\pi} \frac{l_z}{a_{tt}}. \quad (15)$$

For the reasons we discussed earlier in this section, throughout our simulations we focus on inter-trap distances $\eta \geq 1.5$. According to (13), $J(t)$ is practically zero for large η and increases in absolute value, as we bring the traps closer i.e., for decreasing η (see right inset of figure 1). On the contrary, the ground-state frequency $\omega_o(t)$ does not vary appreciably in the same regime of inter-trap distances and thus throughout our simulations we may safely assume that ω_o remains practically constant i.e.,

$$\omega_o(t) \approx \omega_z \left(\frac{1}{2} + \frac{1}{\lambda} \right). \quad (16)$$

Finally, before we proceed further, it is worth recalling here that the two lowest eigenstates of the global double-well potential can be well approximated as the symmetric and antisymmetric combinations of the local eigenstates i.e., $|\pm\rangle = (|A\rangle \pm |B\rangle)/\sqrt{2}$, with eigenfrequencies $\omega_{\pm} = \omega_o \pm J$. Hence, Hamiltonian (8) can be also expressed in terms of the corresponding symmetric and antisymmetric bosonic operators $\hat{d}_{\pm} = (\hat{a} \pm \hat{b})/\sqrt{2}$. (e.g., see [25]). Actually, in some cases one might get further detailed insights into the dynamics of the system if this is viewed in the basis of the global states.

2.3. Outcoupled atoms

Let us assume that atoms are coherently coupled out of the BEC A only. Neglecting collisions between trapped and free atoms, the many-body Hamiltonian for the free atoms is simply of the form [9]

$$\hat{\mathcal{H}}_f = \int d\mathbf{r} \hat{\Psi}_f^\dagger(\mathbf{r}) L_f \hat{\Psi}_f(\mathbf{r}), \quad (17)$$

where

$$L_f = -\frac{\hbar^2}{2m} \nabla^2 + V_f(\mathbf{r}). \quad (18)$$

In general, the potential $V_f(\mathbf{r})$ experienced by the free atoms depends on the particular setup under consideration. Throughout this work we consider an atomic waveguide for the outcoupled atoms [24, 26], resulting in an effective one-dimensional atom laser propagating along the weak confining axis of the waveguide (see figure 1). For instance, such a guided atom laser has been demonstrated recently by Guerin *et al.* [27] and offers many advantages over the conventional outcoupling schemes. Formally speaking, the strong transverse confinement allows us to assume that the transverse dynamics of the free atoms adiabatically follow the slowly varying transverse potential of the optical guide $V_f(\mathbf{r}_\perp)$ [27]. For the sake of simplicity, throughout this work we assume that the transverse guide potential is nearly the same with the transverse potential of trap A i.e., $V_f(\mathbf{r}_\perp) \simeq V_A^{(L)}(\mathbf{r}_\perp)$. In the absence of gravitational or other forces (as in the experimental setup [27]), the longitudinal component of the potential is $V_f(z) = 0$. Thus, the field operator for the free atoms can be expanded as

$$\hat{\Psi}_f(\mathbf{r}, t) = \varphi_A(\mathbf{r}_\perp) \sum_k \chi_k(z) \hat{c}_k(t), \quad (19)$$

where \hat{c}_k is the annihilation operator of free atoms with momentum $\hbar k$ and obeys the usual bosonic commutation relations $[\hat{c}_k, \hat{c}_{k'}^\dagger] = \delta_{k,k'}$. The wavefunction $\varphi_A(\mathbf{r}_\perp)$ is the ground-state wavefunction of the local transverse potential $V_A^{(L)}(\mathbf{r}_\perp)$, with the normalization $\int d\mathbf{r}_\perp |\varphi_A(\mathbf{r}_\perp)|^2 = 1$, so that the linear atomic density $\rho_{1D}(z, t) \equiv \int d\mathbf{r}_\perp |\hat{\Psi}_f(\mathbf{r}, t)|^2 = \sum_{k,q} \chi_k^* \chi_q \hat{c}_k^\dagger \hat{c}_q$. The longitudinal wavefunction $\chi_k(z)$ is readily obtained as a solution of the time-independent Schrödinger equation for a free atom (i.e., for $V_f(z) = 0$). Thus for a free atom with momentum $\hbar k$ we have $\chi_k(z) = e^{ikz}/\sqrt{2\pi}$, and frequency

$$\omega_k = \frac{\hbar k^2}{2m}. \quad (20)$$

As we will see later on, this quadratic dependence of ω_k on k is responsible for a number of mathematical difficulties arising in the context of atom lasers [13]. Using expansion (19) and the orthonormality condition for $\chi_k(z)$, $\hat{\mathcal{H}}_f$ reads

$$\hat{\mathcal{H}}_f = \hbar \sum_k \left(\omega_k + \frac{\omega_z}{\lambda} \right) \hat{c}_k^\dagger \hat{c}_k. \quad (21)$$

2.4. Output coupling

We consider an output coupling by application of external electromagnetic fields which induce an atomic transition from the internal state ($|t\rangle$) of the trapped atoms to an untrapped state $|f\rangle$. In the rotating-wave approximation, the many-body interaction Hamiltonian is of the form [9]

$$\hat{\mathcal{V}}(t) = \hbar \int d\mathbf{r} \hat{\Psi}_f^\dagger(\mathbf{r}) \sqrt{\Lambda(\mathbf{r}, t)} \hat{\Psi}_t(\mathbf{r}) + \text{H.c} \quad (22)$$

where $\Lambda(\mathbf{r}, t)$ is the coupling between trapped and untrapped atomic states. Using the expansions (7) and (19), we obtain

$$\hat{\mathcal{V}}(t) = \frac{\hbar}{\sqrt{2\pi}} \sum_k \hat{c}_k^\dagger \int d\mathbf{r} \sqrt{\Lambda(\mathbf{r}, t)} \varphi_A^*(\mathbf{r}_\perp) e^{-ikz} \left[\varphi_A(\mathbf{r}) \hat{a}(t) + \varphi_B(\mathbf{r}) \hat{b}(t) \right] + \text{H.c} \quad (23)$$

In general the form of $\Lambda(\mathbf{r}, t)$ depends on the particular outcoupling mechanism under consideration. Typical mechanisms may involve one-photon radio-frequency transition or indirect two-photon stimulated Raman transition [7, 8, 9, 11, 12, 26]. Note that in the following we neglect the momentum kick experienced by the atoms as well as the spatial dependence of $\Lambda(\mathbf{r}, t)$, obtaining

$$\hat{\mathcal{V}}(t) = \hbar \sum_k g(k, t) \left(\hat{a} \hat{c}_k^\dagger + \hat{a}^\dagger \hat{c}_k \right) + \hbar e^{-\eta^2} \sum_k g(k, t) \left(\hat{b} \hat{c}_k^\dagger + \hat{b}^\dagger \hat{c}_k \right), \quad (24)$$

where

$$g(k, t) = \frac{\sqrt{l_z}}{\pi^{1/4}} \sqrt{\Lambda(t)} e^{-k^2 l_z^2 / 2}. \quad (25)$$

According to equation (24), the interaction consists of two terms despite the fact that the outcoupling mechanism is applied on BEC A only. More precisely, the first term of $\hat{\mathcal{V}}(t)$ refers to BEC A and is similar to the expression used by many authors in the context of the standard single-mode model for the atom laser [13, 15, 16, 17, 18, 19, 20, 21]. However, due to the presence of the second BEC, in our model we have obtained one more term which is proportional to the overlap of the two ground-state wavefunctions, that is $e^{-\eta^2}$. In that respect, equation (24) is a generalization of the single-mode outcoupling Hamiltonian [13, 15, 16, 17, 18, 19, 20, 21], to a two-mode scenario.

Let us now estimate the spectral response of the atomic continuum for the particular outcoupling mechanism under consideration. The density of states which are available to a free atom can be determined by the dispersion relation (20) as follows

$$\rho(\omega) = \left| \frac{dk}{d\omega} \right| = \sqrt{\frac{m}{2\hbar\omega}} \Theta(\omega), \quad (26)$$

where $\Theta(\omega)$ is the usual step function. Note the divergence of the atomic density of states at the edge frequency $\omega_e = 0$, which is a characteristic property of the one-dimensional model under consideration. Taking advantage of the symmetrical shape

of the coupling and the even parity of ω_k , we may reduce the k -space only to the $k > 0$ sub-space. The spectral response of the continuum is then of the form

$$D(\omega) = 2|g(\omega, t)|^2 \rho(\omega) = \frac{\sqrt{2}\Lambda(t) \exp(-2\omega/\omega_z)}{\sqrt{\pi\omega_z} \sqrt{\omega}} \Theta(\omega), \quad (27)$$

where $g(\omega, t)$ is readily obtained from $g(k, t)$ using the atomic dispersion relation (20).

At this point we have completed the presentation of our model and the underlying approximations. In closing, let us summarize the main results by rewriting the complete form of the Hamiltonian under consideration in a frame rotating at ω_\perp

$$\begin{aligned} \hat{\mathcal{H}} = & \frac{\hbar\omega_z}{2}(\hat{a}^\dagger\hat{a} + \hat{b}^\dagger\hat{b}) + \hbar \sum_k \omega_k \hat{c}_k^\dagger \hat{c}_k + \hbar\kappa(\hat{a}^\dagger\hat{a}^\dagger\hat{a}\hat{a} + \hat{b}^\dagger\hat{b}^\dagger\hat{b}\hat{b}) + \hbar J(\hat{a}^\dagger\hat{b} + \hat{b}^\dagger\hat{a}) \\ & + \hbar \sum_k g(k, t)(\hat{a}\hat{c}_k^\dagger + \hat{a}^\dagger\hat{c}_k) + \hbar e^{-\eta^2} \sum_k g(k, t)(\hat{b}\hat{c}_k^\dagger + \hat{b}^\dagger\hat{c}_k). \end{aligned} \quad (28)$$

3. Heisenberg equations of motion

Given the total Hamiltonian (28) one may proceed to derive Heisenberg equations of motion for the operators of interest. In the Heisenberg picture, the evolution of the expectation value of an arbitrary operator $\hat{\mathcal{A}}$ is governed by

$$\frac{d\langle\hat{\mathcal{A}}\rangle}{dt} = -\frac{i}{\hbar}\langle[\hat{\mathcal{A}}, \hat{\mathcal{H}}]\rangle.$$

Thus, for the operators pertaining to the two traps and the continuum, we obtain

$$\frac{d\langle\hat{a}\rangle}{dt} = -i\frac{\omega_z}{2}\langle\hat{a}\rangle - 2i\kappa\langle\hat{a}^\dagger\hat{a}\hat{a}\rangle - iJ\langle\hat{b}\rangle - 2i \int_0^\infty dk g(k, t)\langle\hat{c}_k\rangle, \quad (29)$$

$$\frac{d\langle\hat{b}\rangle}{dt} = -i\frac{\omega_z}{2}\langle\hat{b}\rangle - 2i\kappa\langle\hat{b}^\dagger\hat{b}\hat{b}\rangle - iJ\langle\hat{a}\rangle - 2ie^{-\eta^2} \int_0^\infty dk g(k, t)\langle\hat{c}_k\rangle, \quad (30)$$

$$\frac{d\langle\hat{c}_k\rangle}{dt} = -i\omega_k\langle\hat{c}_k\rangle - ig(k, t)\langle\hat{a}\rangle - ig(k, t)e^{-\eta^2}\langle\hat{b}\rangle. \quad (31)$$

We may now distinguish between two cases.

In the absence of interatomic interactions (i.e., for $\kappa = 0$) the Hamiltonian (28) becomes bilinear. As a result, the above set of equations is closed and all of the initial statistical properties of the system are preserved in time. For instance, if the BECs are initially in coherent states, we have $\langle\hat{a}^\dagger(t)\hat{a}(t)\rangle = \langle\hat{a}^\dagger(t)\rangle\langle\hat{a}(t)\rangle$, $\langle\hat{b}^\dagger(t)\hat{b}(t)\rangle = \langle\hat{b}^\dagger(t)\rangle\langle\hat{b}(t)\rangle$ and $\langle\hat{c}_i^\dagger(t)\hat{c}_j(t)\rangle = \langle\hat{c}_i^\dagger(t)\rangle\langle\hat{c}_j(t)\rangle$, for all $t \geq 0$ (see also [15, 16, 17, 21]). In other words, the bilinear form of the Hamiltonian preserves the initial coherence in time, so that at any instant t we can decorrelate exactly any higher-order correlation function in terms of $\langle\hat{a}\rangle$, $\langle\hat{b}\rangle$, and $\langle\hat{c}_k\rangle$.

In the presence of interatomic interactions (i.e., for $\kappa \neq 0$) the Hamiltonian (28) involves fourth-order terms, and thus we have the appearance of third-order correlation functions in the right-hand side of equations (29)-(31). This set of equations is no longer closed, while consideration of differential equations for the third-order correlation functions leads to the appearance of terms of even higher order and so on. In general, there are no exact remedies for such mathematical problems, but an approximate solution can be always obtained by decorrelating higher-order correlation functions into products of lower ones.

In the present work we decorrelate the third-order correlation functions appearing on the right-hand side of equations (29)-(31) as follows: $\langle \hat{a}^\dagger \hat{a} \hat{a} \rangle \approx \langle \hat{a}^\dagger \rangle \langle \hat{a} \rangle \langle \hat{a} \rangle$ and $\langle \hat{b}^\dagger \hat{b} \hat{b} \rangle \approx \langle \hat{b}^\dagger \rangle \langle \hat{b} \rangle \langle \hat{b} \rangle$. Hence, equations (29)-(31) read

$$\frac{d\langle \hat{a} \rangle}{dt} = -i\frac{\omega_z}{2}\langle \hat{a} \rangle - 2i\kappa|\langle \hat{a} \rangle|^2\langle \hat{a} \rangle - iJ\langle \hat{b} \rangle - 2i \int_0^\infty dk g(k, t) \langle \hat{c}_k \rangle, \quad (32)$$

$$\frac{d\langle \hat{b} \rangle}{dt} = -i\frac{\omega_z}{2}\langle \hat{b} \rangle - 2i\kappa|\langle \hat{b} \rangle|^2\langle \hat{b} \rangle - iJ\langle \hat{a} \rangle - 2ie^{-\eta^2} \int_0^\infty dk g(k, t) \langle \hat{c}_k \rangle, \quad (33)$$

$$\frac{d\langle \hat{c}_k \rangle}{dt} = -i\omega_k \langle \hat{c}_k \rangle - ig(k, t) \langle \hat{a} \rangle - ig(k, t) e^{-\eta^2} \langle \hat{b} \rangle. \quad (34)$$

One way to solve such a set of coupled differential equations is by means of the Laplace transform method. To this end, however, one has to be able to perform all of the integrations over the continuum as well as the inverse Laplace transforms at the end. Both of these tasks are more or less straightforward in the case of smooth continua for which the Born and Markov approximations are applicable. In the present context, however, none of the aforementioned approximations is valid. Indeed, as we discussed earlier, the quadratic atomic dispersion relation is associated with a density of atomic states which diverges for small frequencies (see equation 26). This behavior is also reflected in the spectral response (27) and implies that the continuum under consideration does not vary slowly for all frequencies.

Structured continua which invalidate both Born and Markov approximations emerge in different areas of physics and have attracted considerable interest over the last few years [1]. To address fundamental mathematical difficulties associated with these continua a number of new theoretical techniques have been developed [1, 19, 28, 29, 30]. Here, to deal with the structured continuum at hand, we follow a discretization approach developed in the context of photonic band-gap continua [31]. Briefly, we substitute the continuum for frequencies within a range around ω_o (i.e., for $0 < \omega < \omega_{up}$), by a number (say M) of discrete modes, while the rest of the atom-mode density is treated perturbatively since it is far from resonance. Discussion on the choice of ω_{up} and the number of discrete modes can be found in Refs. [31]. This approach has been also applied in the context of atom lasers [21], and is capable of providing not only the evolution of the number of atoms in the condensates, but also the distribution of the outcoupled atoms in frequency domain, irrespective of the strength of the outcoupling and the form of the spectral response.

In general, a continuum can be discretized in many different ways (see for instance [21]) and in the present work we have chosen a uniform discretization scheme. In particular, we choose the frequencies of the discrete modes to be $\omega_j = j\varepsilon$, where the mode spacing ε is determined by the upper-limit condition of the discretization, namely $\omega_{up} = M\varepsilon$. The corresponding coupling for the j mode, is determined by the spectral response (27) as follows

$$\tilde{g}_j^2 = D(\omega_j)\varepsilon. \quad (35)$$

Hence, working similarly to [21], equations (32)-(34) read after the discretization

$$\frac{d\langle \hat{a} \rangle}{dt} = -i\left(\frac{\omega_z}{2} - S\right)\langle \hat{a} \rangle - 2i\kappa|\langle \hat{a} \rangle|^2\langle \hat{a} \rangle - i(J - Se^{-\eta^2})\langle \hat{b} \rangle - i \sum_{j=1}^M \tilde{g}_j \langle \hat{c}_j \rangle, \quad (36)$$

$$\frac{d\langle \hat{b} \rangle}{dt} = -i\left(\frac{\omega_z}{2} - Se^{-2\eta^2}\right)\langle \hat{b} \rangle - 2i\kappa|\langle \hat{b} \rangle|^2\langle \hat{b} \rangle - i(J - Se^{-\eta^2})\langle \hat{a} \rangle - ie^{-\eta^2} \sum_{j=1}^M \tilde{g}_j \langle \hat{c}_j \rangle, \quad (37)$$

$$\frac{d\langle\hat{c}_j\rangle}{dt} = -i\omega_j\langle\hat{c}_j\rangle - i\tilde{g}_j\langle\hat{a}\rangle - i\tilde{g}_je^{-\eta^2}\langle\hat{b}\rangle, \quad (38)$$

where

$$S = \int_{\omega_{\text{up}}}^{\infty} \frac{D(\omega)}{\omega} d\omega. \quad (39)$$

4. Simulations

Throughout our simulations we have considered ^{23}Na BECs with $m = 3.818 \times 10^{-26}$ Kgr and $a_{\text{tt}} = 2.75 \times 10^{-9}$ m, which are formed independently in identical harmonic traps with longitudinal oscillation frequency $\omega_z = 200 \text{ sec}^{-1}$ and ratio $\lambda = 0.4$. We assume that the BECs A and B are initially prepared in coherent states $|\alpha\rangle$ and $|\beta\rangle$, respectively. Equations (36)-(38) are thus solved with initial conditions

$$\langle\hat{a}(0)\rangle = \alpha = \sqrt{N\tilde{\alpha}(0)}, \quad \langle\hat{b}(0)\rangle = \beta = \sqrt{N\tilde{\beta}(0)}e^{i\phi(0)}, \quad \langle\hat{c}_j(0)\rangle = 0, \quad (40)$$

where $\phi(0)$ is the initial relative phase between the two BECs. Accordingly, the initial number of condensed atoms in the traps A and B are given by $N_A(0) = |\langle\hat{a}(0)\rangle|^2 = N\tilde{\alpha}(0)$ and $N_B(0) = |\langle\hat{b}(0)\rangle|^2 = N\tilde{\beta}(0)$. At any time $t \geq 0$ we have $\tilde{\alpha}(t) + \tilde{\beta}(t) + \tilde{\gamma}(t) = 1$ so that $N_A(t) + N_B(t) + N_C(t) = N$, where $N_C(t)$ and $\tilde{\gamma}(t)$, respectively are the population and amplitude of the continuum. Finally, for the sake of simplicity and without introducing any significant errors, the applied outcoupling pulse $\Lambda(t)$ is modeled as rectangular lasting from $t = 0$ to $t = \tau$.

Most of the work on the non-Markovian aspects of atom-laser outcoupling has been performed in the framework of an ideal gas (i.e., for $\kappa = 0$) [13, 15, 16, 17, 18, 19, 20, 21]. Hence, for the sake of comparison, in this section we focus mainly on the analysis of results obtained by simulations in non-interacting systems. The case of weakly-interacting gases ($\kappa \neq 0$) deserves a thorough investigation and as such will be discussed in detail elsewhere. At the end of this section, however, we briefly summarize some of the main features of the weakly-interacting systems we have found in our simulations.

4.1. Ideal bosonic gas

As we mentioned earlier, in the absence of interatomic interactions no decorrelation approximations are necessary for the derivation of a closed set of equations for the expectation values of the operators $\langle\hat{a}(t)\rangle$, $\langle\hat{b}(t)\rangle$ and $\langle\hat{c}_j(t)\rangle$. The evolution of the system is obtained by propagating equations (36)-(38) with $\kappa = 0$. As both BECs are assumed initially prepared in coherent states, all of the statistical properties of the system at any time t can be expressed exactly in terms of $\langle\hat{a}(t)\rangle$, $\langle\hat{b}(t)\rangle$ and $\langle\hat{c}_j(t)\rangle$.

4.1.1. Weak outcoupling—Markovian dynamics. As depicted in figure 2, for weak outcoupling strengths (i.e., for $\Lambda < 5 \times 10^2 \text{ sec}^{-2}$), the dynamics of the system are mainly Markovian. More precisely, we have population exchange between the two traps, but the oscillations are exponentially damped as atoms are irreversibly coupled out of the traps. As we reduce the distance η between the traps, the Josephson coupling J increases and the oscillations become faster (e.g., compare figures 2(b) and 2(c)). On the contrary, for constant intertrap distance, the oscillations decay faster as we increase the outcoupling rate Λ (compare figures 2(b) and 2(d)).

In general, the distribution of the outcoupled atoms (see figure 3) exhibits the characteristic doublet which, however, is expected to be asymmetric mainly due to the unconventional density of atomic states (26). In particular, the origin of the doublet is well-described in terms of the global states $|\pm\rangle$ with eigenfrequencies $\omega_z/2 \pm J$. The intertrap coupling splits the previously degenerate local states $|A(B)\rangle$ into a doublet of global states and thus the outcoupled atoms emerge as distinct peaks separated by $2J$. The outcoupling rate is larger for the global state with frequency closer to the edge $\omega_e = 0$, as the density of available atomic states, and thus the spectral response, scales as $1/\sqrt{\omega}$. Decreasing the distance between the two traps, the Josephson coupling increases monotonically for $\eta \leq 2.0$, and thus the distance between the peaks also increases (compare figures 3(b) and 3(c)). On the other hand, as depicted in the inset of figure 1, for $\eta \geq 2.0$ the Josephson coupling is not strong enough to produce a noticeable splitting and to give rise to a clear doublet in the distribution of outcoupled atoms (see figure 3(a)). Finally, as we increase the outcoupling rate Λ for constant η , the peaks become broader while their position remains practically unchanged (compare figures 3(b) and 3(d)).

4.1.2. Strong outcoupling—Non-markovian dynamics. In the strong-outcoupling regime (i.e., for $\Lambda \geq 5 \times 10^2 \text{ sec}^{-2}$) the trapped populations begin exhibiting non-Markovian dynamics. In general, the evolution of the system is governed by two different processes namely, the exchange of population between the BECs and the exchange of population between the BECs and the continuum. Note that exchange of population between any discrete feature and a continuum is a signature of the non-Markovian nature of the problem under consideration.

In figure 4 we present the evolution of the trapped populations as functions of time, for a given intertrap distance and increasing outcoupling rate. Clearly, as far as trap B is concerned, we can identify an initial transient regime where the main part of the population is lost. After this initial stage, dissipation is temporarily turned off and trap B gets atoms from trap A (slight oscillations). This weak oscillatory population exchange between the two traps persists even for larger times, but the population of trap B is gradually transferred into the continuum in an *irreversible*, almost exponential, way. Thus, irrespective of the strength of the outcoupling rate, trap B is always empty in the long-time limit (e.g., see figures 4(a,b)).

Moreover, in figure 4 we see that, besides the weak oscillations, the population of trap A exhibits fast oscillations which become more pronounced and faster with increasing outcoupling strength. These oscillations are reflected only in the population of the continuum which is not shown here. For relatively weak outcoupling rates not only trap B, but also trap A is empty in the long-time limit (e.g., see figures 4(a,b)). On the contrary, for stronger outcoupling rates the system reaches a steady state pertaining to a practically empty trap B and a partly depleted BEC A (e.g., see figures 4(d)). The formation of such a *bound state* has been demonstrated experimentally [14] and involves atoms in a *superposition* of two states namely, the trapped and the untrapped state. The Born and Markov approximations are valid only if such superpositions decay on a time scale much shorter than the time scale of interest in this work. It is also worth noting that, according to our simulations (e.g., see figure 4), the bound state involves only trap A and not trap B. This is perhaps due to the weak outcoupling rate for BEC B which is proportional to the overlap $e^{-\eta^2}$ between the two BEC wavefunctions. Hence, BEC B is only weakly coupled to the continuum and any non-Markovian effects, such as the formation of a bound state, are suppressed.

Finally, although limitations in the validity of the two-mode model does not allow us to consider larger values of Λ , from figure 5(a) it is obvious that the population trapping increases as we increase the outcoupling rate.

Let us discuss now the effect of the intertrap distance η on the evolution of the trapped populations. As depicted in figure 6 (a), for large intertrap distances the weak oscillations are absent and the population of trap B remains practically constant as the overlap between the BEC wavefunctions is negligible. As we bring the traps closer (see figures 6 (b-d)), the population of trap B starts evolving in time with an initial transient regime followed by an irreversible decay. On the other hand, for the typical values of η allowed by our two-mode approximation, there seems to be no significant effect on the evolution of the population of trap A. In particular, we have a continuous exchange of population between trap A and the continuum until the formation of a bound state in the long-time limit. Although the steady-state population of trap A does not change considerably over the regime of intertrap distances η we can cover, a slight reduction is noticeable in figure 5(b) as we reduce η . Moreover, there is a regime of distances around $\eta_c \approx 2.14$, where the system seems to have no steady state, in the conventional sense of the word, as it is beating between the two localized condensate modes even for the long time scale used in figure 5. That is why we do not give any values for $\langle \hat{a}^\dagger(\tau)\hat{a}(\tau) \rangle$ in the neighborhood of η_c . All of this behavior can be easily understood if the system is viewed in the basis of the symmetric and antisymmetric global states $|\pm\rangle$.

First of all let us briefly discuss the behavior of the global states $|\pm\rangle$ with eigenenergies $\omega_\pm = \omega_z/2 \pm J$, as we approach the two traps. As depicted in the inset of figure 1, the Josephson coupling and thus the separation of the global states, does not vary monotonically with η . More precisely, as we reduce η the splitting of the states $|\pm\rangle$ increases for $\eta \geq \eta_{\min}$, where $\eta_{\min} \approx 2.3$. In this regime of intertrap distances, J is negative and thus $\omega_- > \omega_+$ i.e., the symmetric state moves to the left and the antisymmetric state to the right of the characteristic frequency $\omega_z/2$. This relative movement is inverted for $\eta_c < \eta < \eta_{\min}$ and the two global states begin approaching each other. They become basically resonant at $\eta = \eta_c$ where J changes sign. Subsequently, as we further reduce η , the splitting of the states $|\pm\rangle$ increases again, but this time the global states move in opposite directions as $J > 0$ and $\omega_+ > \omega_-$. In particular, the symmetric state moves away from the edge and the population trapping associated with it decreases, whereas the antisymmetric state moves towards the edge where it is more protected against dissipation. In any case, it is worth noting that the Josephson coupling attains significant values only for $\eta < 2.0$. Thus, for $2.0 < \eta < 3.0$ the two condensate modes are practically resonant, as the splitting is negligible. Hence, the system is beating between the two condensate modes and no steady-state is found on the time scale of figure 5.

In view of the above discussion, it is also easy to understand the reduction of the steady-state population of trap A as we bring the traps closer. For the particular initial conditions under consideration, we obtain $\langle d_+^\dagger(0)d_+(0) \rangle = |\alpha + \beta|^2/2$ and $\langle d_-^\dagger(0)d_-(0) \rangle = |\alpha - \beta|^2/2$. Throughout this work we have focused on in-phase BECs only i.e., $\phi = 0$. As a result, the main part of the population initially occupies the symmetric global state and thus the behavior of the corresponding steady-state population with decreasing η also determines the behavior of the steady-state population in the local state $|A\rangle$. This may not be the case if we choose different initial conditions, but the effect of the phase difference ϕ on the system's dynamics will be investigated in detail elsewhere.

We turn now to the discussion of the distribution of the outcoupled atoms in the non-Markovian regime. Unfortunately, for the spectral response (27) the derivation of analytic expressions for the atomic distribution is a rather difficult task [16]. In fact, analytic results can be obtained only in some special cases e.g., in the limit of broad-band output coupling, by means of the Laplace transform method [16]. The discretization approach, however, is capable of providing us with the distribution of the outcoupled atoms at any time. In figures 7 and 8 we present such typical distributions at the end of the outcoupling pulse, i.e. at times $t = \tau$, with the pulse duration chosen sufficiently large to ensure that the distributions do not vary significantly with time.

For a better interpretation of these results, it is worth keeping in mind that the system under consideration involves two condensate modes which decay into the same atomic continuum. Moreover, there are two different outcoupling channels for each mode. More precisely, atoms can be coupled out of BEC A either directly or via BEC B and vice-versa; albeit at different rates. As a result we expect quantum interference effects which in addition to the non-Markovian nature of the dynamics may give rise to unconventional distributions of the outcoupled atoms.

When the traps are far apart (see figure 7(a)), we are essentially in the single-trap case where atoms are coherently outcoupled from BEC A only. In this case any quantum interference effects are absent and the distribution of the outcoupled atoms exhibits a well-known profile previously discussed in Ref. [21]. More precisely, we have a peak around the condensate-mode frequency $\omega_z/2$, and a peak around the edge frequency $\omega_e = 0$ where the density of atomic states diverges (see equation 26). The former peak is shifted towards higher frequencies due to the coupling between the condensate mode and the continuum. This effect has also been noted by other authors (e.g., see [20]) and becomes more pronounced as we increase the outcoupling rate. Moreover, the time-dependence of the presented distributions gives rise to oscillations which become faster as we increase the pulse duration. In the Markovian regime, the atomic distributions do not exhibit any such oscillations (see figure 3) as all of the time-dependent terms entering the distributions become practically negligible for times $At \gg 1$. In the non-Markovian regime, however, we have a continuous exchange of atoms between the BECs and the continuum even for larger times as well as the formation of a non-decaying bound mode in the long-time limit. Hence, there exist time-dependent terms associated with the formed bound mode which persist even in the limit $t \rightarrow \infty$ and their effect on the atomic distribution is evident, unless one performs a time average over the period of the oscillations (see also discussion in [32, 33]).

As the traps approach each other (see figure 7(b)), the overlap between the two BECs increases and a narrow peak appears next to the main peak. This narrow peak is clearly associated with a rather weak outcoupling and thus can be attributed to atoms originated from trap B. It could be said therefore that for intermediate intertrap distances the distribution of the outcoupled atoms is basically a superposition of the distributions for each individual trap. As we reduce further the intertrap distance η , quantum interference effects start becoming significant, and a clear dip appears next to the narrow peak (see figures 7(c,d)).

As depicted in figure 8(a), the dip is also present for relatively weak outcoupling strengths provided the two traps are close enough. Actually, it was also present in the Markovian regime (see figure 3), but it was not so clear as the two peaks were far apart. It is obvious therefore that the dip is a clear evidence of destructive interference between the various outcoupling channels of the system. Although the outcoupling

itself is not sufficient to cause the dip, in figure 9 we see that the dip becomes broader with increasing outcoupling rates, while one may also notice the emergence of the narrow peak at frequencies around $\omega_z/2$ in figures 8(b)-(d).

Due to the lack of analytic expressions, it is not clear whether the observed dip at $\omega_j \equiv \omega_d$ is a perfect dark line i.e, whether $\langle \hat{c}_j^\dagger(\tau) \hat{c}_j(\tau) \rangle = 0$ at ω_d . To resolve this issue we have obtained analytic expressions for the distributions in the broad-band limit of the output coupling where $D(\omega) \sim \Lambda(t)/\sqrt{\omega}$ [13, 16]. In this limit, the observed profiles are similar to the ones presented here and we can verify that the atomic distribution at $\omega_j = \omega_d$ vanishes only in the limit $t \rightarrow \infty$. Otherwise, for $\Lambda t \gg 1$ the dip corresponds to a very low probability ($\sim 10^{-6}$) for outcoupled atoms with frequency ω_d .

4.2. Weakly-interacting bosonic gas

Considering a harmonic trap with longitudinal oscillation frequency $\omega_z = 200\text{sec}^{-1}$ and ratio $\lambda = 0.4$, condition (15) yields $N \ll 2.5 \times 10^3$. In other words, our model is valid for small BECs consisting of a few hundred of atoms. As we discussed in section 3, in the presence of interactions we can obtain a closed set of equations of motion for the operators $\langle \hat{a}(t) \rangle$, $\langle \hat{b}(t) \rangle$ and $\langle \hat{c}_j(t) \rangle$, only by applying a decorrelation approximation. In view of this decorrelation, interatomic interactions enter the equations of motion for $\langle \hat{a}(t) \rangle$ and $\langle \hat{b}(t) \rangle$ as time-dependent shifts proportional to the corresponding trapped populations $N_A(t) = |\langle \hat{a}(t) \rangle|^2$ and $N_B = |\langle \hat{b}(t) \rangle|^2$ (see equations 36 and 37). As a result, the frequencies of the condensate modes A and B fluctuate in time and become off-resonant.

The evolution of the weakly interacting system is governed by three distinct physical processes. More precisely, apart from the Josephson and the output coupling which were also present in the interaction-free model, we also have the repulsive collisional interactions. It is reasonable therefore to define the ratios $N_c^{(t)} = J/\kappa$ and $N_c^{(f)} = \sqrt{\Lambda}/\kappa$ which quantify the effect of interatomic interactions relative to tunneling and outcoupling effects, respectively. How strongly the inclusion of interactions affects the results obtained in the framework of the interaction-free model depends on the ratios $N/N_c^{(t)}$ and $N/N_c^{(f)}$, where N is the total number of atoms in the system.

The case of weakly-interacting gases is of particular interest but it cannot be covered in the present work as there are many aspects which need to be thoroughly investigated. For instance, it is already known that for an isolated double-well BEC (i.e., in the absence of losses and outcoupling) one may define two extreme regimes of dynamics [34] namely the Josephson regime [35] and the self-trapping regime [34]. The detailed analysis of the previous section does not involve self-trapping at all as this phenomenon occurs only for Hamiltonians involving interactions. Here, we would like to briefly highlight only some of the features of the weakly-interacting model we have found in our simulations. The detailed presentation and discussion of the results will be the subject of a forthcoming work.

In the strong outcoupling regime (i.e., for $N_c^{(f)} > N$), inclusion of interactions affects the evolution of the trapped populations only quantitatively. The most important features of the weakly-interacting system in this regime seem to be the destruction of the bound mode and the disappearance of the dark spectral line discussed in the context of the interaction-free model. On the other hand, for $N_c^{(f)} < N$ interatomic interactions dominate over the output coupling and thus we have strong

modifications in the evolution of the populations as well as the distribution of the outcoupled atoms.

5. Summary and outlook

We have investigated the non-Markovian aspects of atom-laser outcoupling from a double-well BEC. Our two-mode trapped condensate model has been motivated by recent experiments on the merging of independently formed BECs [4], and the first realization of a guided quasicontinuous atom laser [27]. For the sake of comparison with earlier work, relying on a single-mode trapped condensate, we have focused on an interaction-free model. In particular, we have studied how the presence of the second BEC (BEC B) affects the evolution of the trapped populations as well as the distribution of the outcoupled atoms. Although the outcoupling mechanism is basically applied only to BEC A, atoms are also weakly outcoupled from BEC B due to the overlap between the BEC wavefunctions.

In the case of weak outcoupling rates the dynamics of the system are purely Markovian and thus particularly simple. More precisely, the system oscillates between the two condensate modes while atoms are coherently outcoupled into the continuum. The distribution of the outcoupled atoms exhibits the characteristic asymmetric doublet due to the unconventional density of atomic states and the different outcoupling rates experienced by the BEC atoms.

The situation is substantially different in the strong-outcoupling regime, where the system exhibits non-Markovian dynamics. In particular, we have population exchange between the two BECs as well as between the BECs and the continuum. In the latter process, BEC B seems to participate passively as its population is gradually transferred to the continuum in an irreversible way. On the contrary, BEC A keeps exchanging population with the continuum even for larger times while for sufficiently strong outcoupling rates it is found only partially depleted in the long-time limit. The formation of such a bound state has also been predicted in the context of single-mode models. However, in the two-mode model under consideration the long-time-limit behavior of the system seems to depend on several parameters such as the outcoupling rate, the intertrap distance and the phase difference between the two BECs.

The non-Markovian nature of the dynamics and the presence of the second BEC are mostly apparent in the distribution of the outcoupled atoms which exhibits two peaks. On the one hand, there is a broad peak stemming from atoms directly outcoupled from BEC A while on the other hand, atoms outcoupled from BEC B give rise to a rather narrow peak. Most importantly, as a result of destructive quantum interference between various outcoupling channels in the system, the atomic distribution may also exhibit a dark spectral line. It is worth noting that similar quantum interference phenomena have been discussed in the context of optical systems. Nevertheless, to the best of our knowledge the appearance of dark lines in the spectrum of atom lasers has not been discussed in the literature so far.

In general, the two-mode model considered here allows for the direct inclusion of collisional interactions between trapped atoms. Nevertheless, due to space limitations, throughout this work we have focused on an interaction-free model only, and have assumed that the two BECs are initially in phase. Effects of interactions and the role of the phase difference will be presented in detail elsewhere.

Acknowledgments

The authors thank David Petrosyan for his critical reading of the manuscript.

References

- [1] Breuer H P and Petruccione F 2002 *The Theory Of Open Quantum Systems* (Oxford University Press)
- [2] Lambropoulos P, Nikolopoulos G M, Nielsen T R and Bay S 2000 *Rep. Prog. Phys.* **63** 455
- [3] Spreeuw R J C, Pfau T, Janicke U and Wilkens M 1995 *Europhys. Lett.* **32** 469; Holland M, Burnett K, Gardiner C, Cirac J I and Zoller P 1996 *Phys. Rev. A* **54** R1757; Santos L, Floegel F, Pfau T and Lewenstein M 2001 *Phys. Rev. A* **63**, 063408; Mandonnet E, Minguzzi A, Dum R, Carusotto I, Castin Y and Dalibard J 2000 *Eur. Phys. J. D* **10**, 9
- [4] Chikkatur A P, Shin Y, Leanhardt A E, Kielpinski D, Tsikata E, Gistavson T L, Pitchard D E and Ketterle W 2003 *Science* **282** 2193
- [5] Wiseman H, Martins A and Walls D 1996 *J. Opt. B: Quant. Semiclass. Opt.* **8** 737; Wiseman H M, Burnett K and Collett M J 1999 *J. Phys. B* **32** 3669
- [6] Guzman A, Moore M and Meystre P 1996 *Phys. Rev. A* **53** 977; Zobay O and Meystre P 1998 *Phys. Rev. A* **57** 4710
- [7] Ballagh R J, Burnett K and Scott T F 1997 *Phys. Rev. Lett* **78** 1607
- [8] Jackson B, McCann J F and Adams C S 1998 *J. Phys. B* **31** 4489
- [9] Japha Y, Choi S and Burnett K 2000 *Phys. Rev. A* **61** 063606
- [10] Robins N, Savage C and Ostrovskaya E A 2001 *Phys. Rev. A* **64** 043605; S.A. Haine S A, Hope J J, Robins N P and Savage C M 2002 *Phys. Rev. Lett.* **88** 170403
- [11] Graham R and Walls D F 1999 *Phys. Rev. A* **60** 1429
- [12] Edwards M, Griggs D A, Holman P L, Clark C W, Rolston S L and Phillips W D 1999 *J. Phys. B* **32** 2935
- [13] Moy G M, Hope J J and Savage C M 1999 *Phys. Rev. A* **59** 667
- [14] Robins N P, Morrison A K, Hope J J and Close J D 2005 *Phys. Rev. A* **72** 031606(R)
- [15] Hope J J 1997 *Phys. Rev. A* **55** R2531
- [16] Moy G M and Savage C M 1997 *Phys. Rev. A* **56** R1087
- [17] Hope J J, Moy G M, Collett M J and Savage C M 2000 *Phys. Rev. A* **61** 023603
- [18] Jack M W, Naraschewski M, Collett M J and Walls D F 1999 *Phys. Rev. A* **59** 2962
- [19] Breuer H P, Faller D, Kappler B and Petruccione F 1999 *Phys. Rev. A* **60** 3188
- [20] Jeffers J, Horak P, Barnett S M and Randmore P M 2000 *Phys. Rev. A* **62** 043602
- [21] Nikolopoulos G M, Lambropoulos P and Proukakis N P 2003 *J. Phys. B* **36**, 2797
- [22] Yi W and Duan L-M 2005 *Phys. Rev. A* **71** 043607
- [23] Mebrahtu A, Sanpera A and Lewenstein M 2006 *Phys. Rev. A* **73** 033601
- [24] Meystre P 2001 *Atom Optics* (New York: Springer Verlag)
- [25] Javanainen J and Ivanov M Y 1999 *Phys. Rev. A* **60** 2351; Milburn G J, Corney J, Wright E M and Walls W F 1997 *Phys. Rev. A* **55** 4318
- [26] Moy G M, Hope J J and Savage C M 1997 *Phys. Rev. A* **55** 3631
- [27] Guerin W, Riou J-F, Gaebler J P, Josse V, Bouyer P and Aspect A 2006 *Phys. Rev. Lett.* **97** 200402
- [28] Strunz W T, Diosi L and Gisin N 1999 *Phys. Rev. Lett* **82** 1801; Diosi L, Gisin N and Strunz W T 1998 *Phys. Rev. A* **58** 1699 (1998)
- [29] Garraway B M 1997 *Phys. Rev. A* **55** 2290; Dalton B J, Barnett S M, and Garraway B M 2001 *Phys. Rev. A* **64** 053813
- [30] Jack M W and Hope J J 2001 *Phys. Rev. A* **63** 043803
- [31] Nikolopoulos G M, Bay S and Lambropoulos P 1999 *Phys. Rev. A* **60** 5079; Nikolopoulos G M and Lambropoulos P 2000 *Phys. Rev. A* **61** 053812
- [32] Bay S, Lambropoulos P and Mølmer K 1997 *Phys. Rev. A* **55** 1485
- [33] Eberly J H and Wódkiewicz K 1977 *J. Opt. Soc. Am.* **67** 1252
- [34] Albiez M, Gati R, Fölling J, Hunsmann S, Cristani M and Markus M K 2005 *Phys. Rev. Lett.* **95** 010402; Smerzi A, Fantoni S, Giovanazzi S and Shenoy S R 1997 *Phys. Rev. Lett.* **79** 4950
- [35] Javanainen J 1986 *Phys. Rev. Lett.* **57** 3164

Figure captions

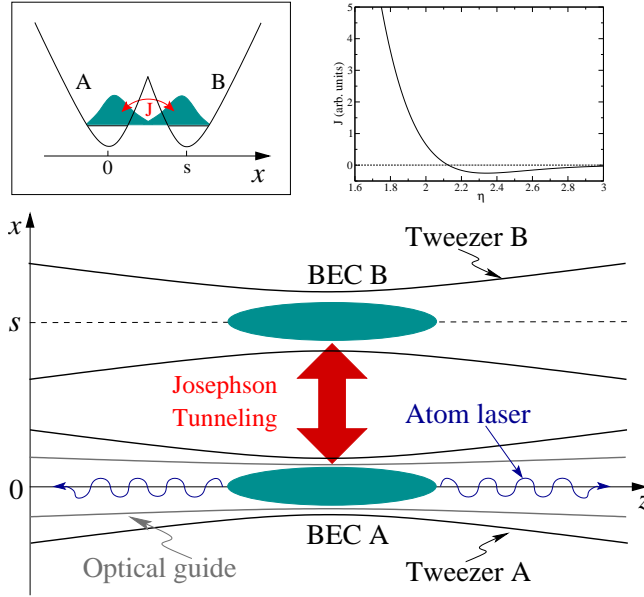


Figure 1. Schematic representation of the system under consideration. Left inset: The double-well potential experienced by the trapped atoms along the x -direction. Right inset: The Josephson coupling as a function of the dimensionless intertrap distance η .

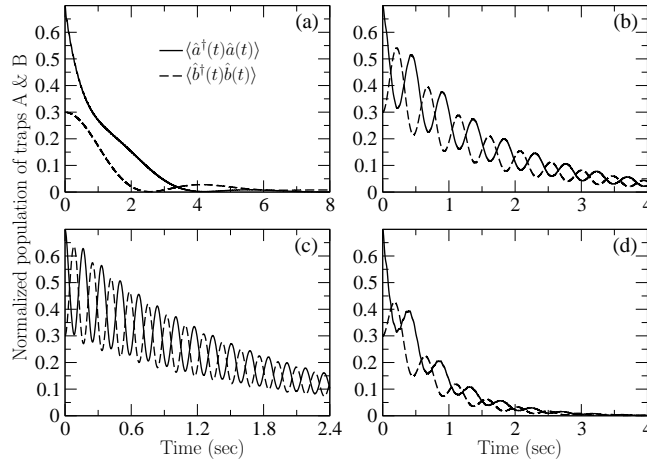


Figure 2. Markovian regime. Evolution of the normalized trap populations as a function of time for various inter-trap distances and outcoupling strengths: (a) $\Lambda = 10^2 \text{ sec}^{-2}$, $\eta = 2.0$; (b) $\Lambda = 10^2 \text{ sec}^{-2}$, $\eta = 1.7$; (c) $\Lambda = 10^2 \text{ sec}^{-2}$, $\eta = 1.5$; (d) $\Lambda = 2 \times 10^2 \text{ sec}^{-2}$, $\eta = 1.7$. System parameters: $\omega_z = 200 \text{ sec}^{-1}$, $\lambda = 0.4$. Initial conditions: $\tilde{\alpha}(0) = 0.7$, $\tilde{\beta}(0) = 0.3$. Discretization parameters: $M = 1500$, $\omega_{\text{up}} = 300 \text{ sec}^{-1}$.

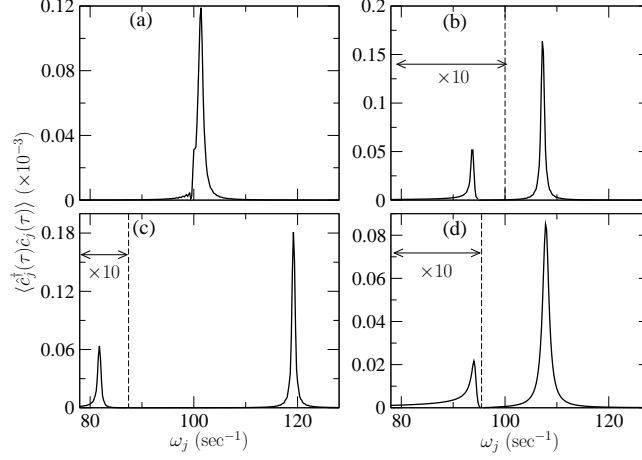


Figure 3. Markovian regime. Distribution of the outcoupled atoms at $\tau = 10$ sec for various inter-trap distances and outcoupling strengths. The distributions (a)-(d) are in one-to-one correspondence with figures 2(a)-(d), respectively. Note that for the sake of illustration the regime on the left-hand side of the vertical dashed line has been magnified ten times.

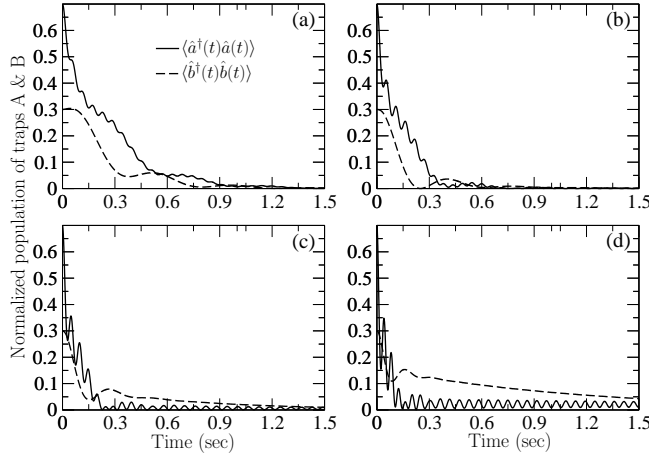


Figure 4. Non-markovian regime. Evolution of the normalized trap populations as a function of time for various outcoupling strengths: (a) $\Lambda = 5 \times 10^2 \text{ sec}^{-2}$; (b) $\Lambda = 10^3 \text{ sec}^{-2}$; (c) $\Lambda = 2 \times 10^3 \text{ sec}^{-2}$; (d) $\Lambda = 4 \times 10^3 \text{ sec}^{-2}$. System parameters: $\omega_z = 200 \text{ sec}^{-1}$, $\lambda = 0.4$, $\eta = 1.7$. Initial conditions: $\tilde{\alpha}(0) = 0.7$, $\tilde{\beta}(0) = 0.3$. Discretization parameters: $M = 1500$, $\omega_{\text{up}} = 300 \text{ sec}^{-1}$.

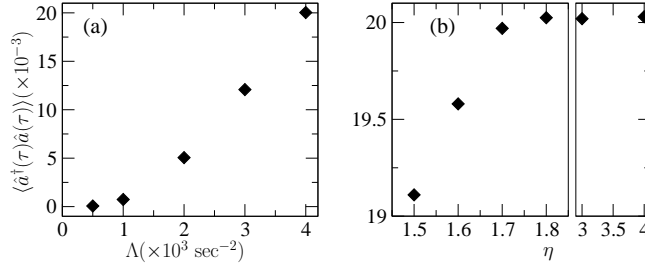


Figure 5. Non-markovian regime. Typical behavior of the steady-state population of trap A for varying outcoupling rate (a) and dimensionless intertrap distance (b). The depicted values are estimated numerically for a sufficiently dense discretization and pulse duration $\tau = 40$ sec. In the neighborhood of $\eta \approx 2.14$, we have not found a steady-state for trap A, although we have let the system evolve for times up to $\tau = 50$ sec. System parameters: $\omega_z = 200 \text{ sec}^{-1}$, $\lambda = 0.4$, $\eta = 1.7$ for plot (a) and $\Lambda = 4 \times 10^3 \text{ sec}^{-2}$ for plot (b). Initial conditions: $\tilde{\alpha}(0) = 0.7$, $\tilde{\beta}(0) = 0.3$. Discretization parameters: $M = 3000$, $\omega_{\text{up}} = 300 \text{ sec}^{-1}$.

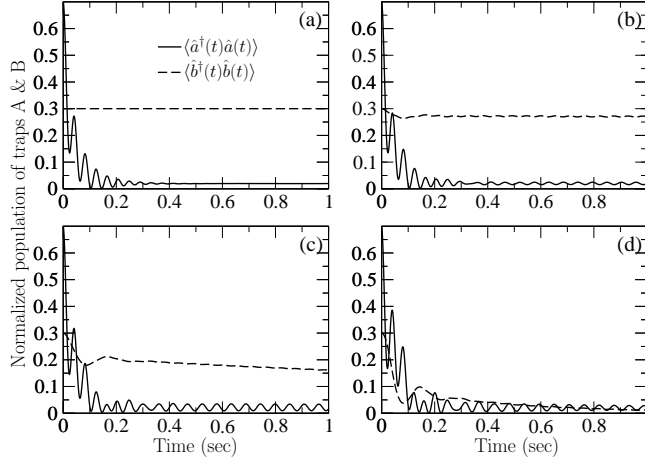


Figure 6. Non-markovian regime. Evolution of the normalized trap populations as a function of time for various inter-trap distances: (a) $\eta = 4.0$; (b) $\eta = 2.0$; (c) $\eta = 1.8$; (d) $\eta = 1.6$. System parameters: $\omega_z = 200 \text{ sec}^{-1}$, $\lambda = 0.4$, $\Lambda = 4 \times 10^3 \text{ sec}^{-2}$. Initial conditions: $\tilde{\alpha}(0) = 0.7$, $\tilde{\beta}(0) = 0.3$. Discretization parameters: $M = 1500$, $\omega_{\text{up}} = 300 \text{ sec}^{-1}$.

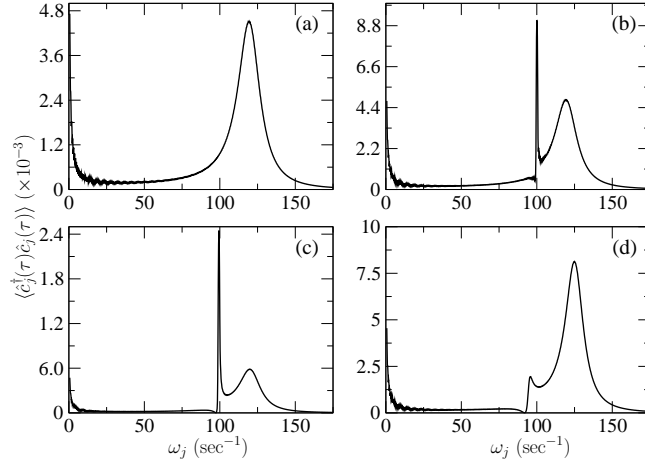


Figure 7. Non-markovian regime. Distribution of the outcoupled atoms at $\tau = 10$ sec for $\Lambda = 2 \times 10^3 \text{ sec}^{-2}$ and various inter-trap distances: (a) $\eta = 4.0$; (b) $\eta = 2.0$; (c) $\eta = 1.8$; (d) $\eta = 1.6$. System parameters: $\omega_z = 200 \text{ sec}^{-1}$, $\lambda = 0.4$, $\Lambda = 2 \times 10^3 \text{ sec}^{-2}$. Initial conditions: $\tilde{\alpha}(0) = 0.7$, $\tilde{\beta}(0) = 0.3$. Discretization parameters: $M = 1500$, $\omega_{\text{up}} = 300 \text{ sec}^{-1}$.

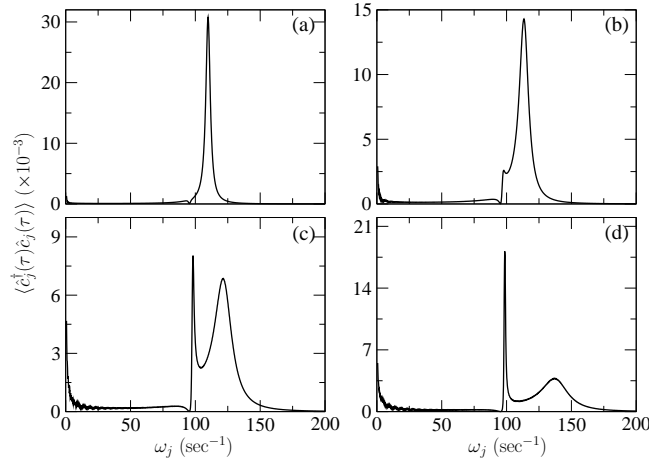


Figure 8. Non-markovian regime. As in figure 7 for $\eta = 1.7$ and various outcoupling strengths: (a) $\Lambda = 5 \times 10^2 \text{ sec}^{-2}$; (b) $\Lambda = 10^3 \text{ sec}^{-2}$; (c) $\Lambda = 2 \times 10^3 \text{ sec}^{-2}$; (d) $\Lambda = 4 \times 10^3 \text{ sec}^{-2}$.

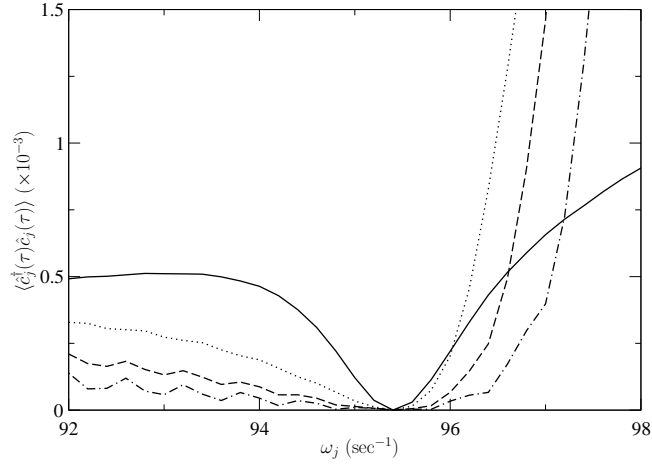


Figure 9. Non-markovian regime. A closeup of the atomic distribution around the dip for the parameters of figure 8 and various outcoupling strengths: $\Lambda = 5 \times 10^2 \text{ sec}^{-2}$ (solid line), $\Lambda = 10^3 \text{ sec}^{-2}$ (dotted line), $\Lambda = 2 \times 10^3 \text{ sec}^{-2}$ (dashed line), and $\Lambda = 4 \times 10^3 \text{ sec}^{-2}$ (dot-dashed line).